NeuroImage: Clinical 28 (2020) 102425

Contents lists available at ScienceDirect

NeuroImage: Clinical

journal homepage: www.elsevier.com/locate/ynicl

The structural basis for interhemispheric functional connectivity: Evidence from individuals with agenesis of the corpus callosum

Junliang Yuan[a,c,d,f,1], Xiaopeng Song[a,b,c,1], Elliot Kuan[b,c], Shuangkun Wang[e], Long Zuo[e], Dost Ongur[b,c], Wenli Hu[d,*], Fei Du[a,b,c,*]

[a] McLean Imaging Center, McLean Hospital, 02478, United States
[b] Psychotic Disorders Division, McLean Hospital, 02478, United States
[c] Harvard Medical School, Boston, MA 02115, United States
[d] Department of Neurology, Beijing Chaoyang Hospital, Capital Medical University, Beijing 100020, China
[e] Department of Radiology, Beijing Chaoyang Hospital, Capital Medical University, Beijing 100020, China
[f] National Clinical Research Center for Mental Disorders, Peking University Sixth Hospital, Beijing 100191, China

ARTICLE INFO

Keywords:
Corpus callosum
Functional magnetic resonance imaging
Functional connectivity
Voxel-mirrored homotopic connectivity
Diffusion tensor imaging
Structural connectivity

ABSTRACT

Agenesis of the corpus callosum (AgCC) is a rare congenital malformation characterized by partial or complete absence of the corpus callosum (CC). The effects of AgCC on cerebral structural and functional networks are not clear. We aimed to utilize AgCC as a model to characterize the relationship between brain structure and function. Diffusion tensor imaging and resting-state fMRI data were collected from nine AgCC and ten healthy subjects. The interhemispheric functional connectivity (FC) was quantified using a voxel-mirrored-homotopic-connectivity (VMHC) method, and its correlation with the number (FN) and fractional anisotropy (FA) of the fibers crossing the CC was calculated. Graph-based network analyses of structural and functional topologic properties were performed. AgCC subjects showed markedly reduced VMHC compared to controls. VMHC was significantly correlated with the FN and FA of the fibers crossing the CC. Structural network analyses revealed impaired global properties, but intact local properties in AgCC compared to controls. Functional network analyses showed no significant difference in network properties between the groups. Finally, in both groups, brain areas with more fiber connections were more likely to build a positive FC with each other, while areas with decreased white matter connections were more likely to result in negative FC. Our observations demonstrate that interhemispheric FC is highly dependent on CC structure. Increased alternative intrahemispheric SC might be a compensatory mechanism in AgCC that helps to maintain normal global brain function. Our study provides insights into the underlying neurological pathophysiology of brain malformations, thereby helping to elucidate the structure–function relationship of normal human brain.

1. Introduction

The relationship between brain function and structure has been studied for decades (Park and Friston, 2013), yet many questions remain unanswered, e.g. how rich functionality emerges from the structural architecture of the brain. Non-invasive magnetic resonance imaging (MRI) has provided insights into the association between brain structure and function. Diffusion tensor imaging (DTI) (Le Bihan et al., 2001) and resting-state functional MRI (rs-fMRI) (Biswal, 2012) are two MRI procedures that can measure brain structure and function respectively. DTI captures the molecular diffusion of water along white matter fibers and thereby provides a measure of white matter structures (namely structural connectivity, SC). Rs-fMRI can measure the statistical properties of the neural activities from different brain regions (i.e. functional connectivity, FC). FC has previously been shown to correlate with SC at an aggregate level both in healthy controls (HC) (Honey et al., 2009) and in disease conditions (Kozel et al., 2011; Miguel-Hidalgo, 2013). Although it is intuitive that functional networks rely on the structural network (Straathof et al., 2019), it is still unclear to what extent FC is determined by SC (O'Reilly et al., 2013; Park and Friston, 2013).

The corpus callosum (CC) is the largest white matter structure connecting the two brain hemispheres. Therefore, it is reasonable to assume that the CC may play a major role in maintaining homotopic FC

* Corresponding authors at: McLean Imaging Center, McLean Hospital, Harvard Medical School, Belmont, MA 02478, United States.
E-mail addresses: wenlihu3366@126.com (W. Hu), fdu@mclean.harvard.edu (F. Du).
[1] Junliang Yuan and Xiaopeng Song contributed equally to this work.

https://doi.org/10.1016/j.nicl.2020.102425
Received 2 April 2020; Received in revised form 20 August 2020; Accepted 25 August 2020
Available online 15 September 2020

in the brain. Agenesis of corpus callosum (AgCC) is a rare congenital malformation in which callosal fibers are congenitally partially or fully absent and is caused by different genetic or environmental factors during prenatal development (Calabrò et al., 2015; Paul et al., 2007). Thus, AgCC can serve as a good neuroanatomical model for understanding human neuroplasticity and the relationship between SC and FC in certain developmental abnormalities (Meoded et al., 2015; Tovar-Moll et al., 2007).

Despite the dramatic differences in white matter structure, several prior studies found no significant difference in basic cognition and intelligence between AgCC subjects and HC (Calabrò et al., 2015; Paul et al., 2007). Rs-fMRI studies also found that global FC was nearly intact in AgCC (Owen et al., 2013a; Tyszka et al., 2011), indicating that indirect or local polysynaptic pathways were utilized to preserve remote FC in AgCC subjects (Owen et al., 2013a; Tyszka et al., 2011). However, the actual functional-structural changes involved in this disease are still unknown (Roland et al., 2017). For instance, what brain areas are mainly connected by the corpus callosum (CC) in the healthy brain? Would these brain areas show decreased inter-hemispheric or homotopic FC with impaired CC? If they do, does the extent of homotopic FC disruption reflect the proportion of anatomical impairment?

To address these issues, we adopted a voxel-mirrored homotopic connectivity (VMHC) approach (Mancuso et al., 2019; Tovar-Moll et al., 2014) to examine interhemispheric functional synchrony and to investigate its relationship with structural properties, indicated by the number (FN) and fractional anisotropy (FA) of the CC fibers in both AgCC and HC. We identified the structural connections that are highly reliant on the CC by probabilistic tractography and explored the dependency of FC on SC. Lastly, we used topographic theory on DTI and rs-fMRI data to study the global SC and FC at the network level in AgCC and HC. VMHC quantifies the FC between each voxel in one hemisphere and its mirrored counterpart in the other hemisphere (Hung et al., 2019; Owen et al., 2013b; Ridley et al., 2016). Graph-based approaches model the brain as a complex network represented graphically by a collection of nodes and edges. In the virtual graph, nodes indicate anatomical elements (e.g., brain regions) and edges represent the relationships between nodes (e.g., connectivity) (Wang et al., 2010). After the network modeling procedure, various graph theoretical metrics can be used to investigate the organizational configuration of the brain networks (Wang et al., 2015, 2010). Since the VMHC method quantifies inter-hemispheric FC in a voxel-wise manner, while traditional graph-based network analysis quantifies the overall connectivity pattern among all the regions of the brain and characterizes the global organization of the whole brain, VMHC might be more sensitive than graph-based approaches in this case. In addition to investigating the structural and functional deficits in AgCC subjects, our main goal was to reveal the general relationship between FC and SC. We hypothesized that: 1) the VMHC method would reveal interhemispheric FC changes in AgCC that traditional graph-based methods failed to detect; 2) disrupted homotopic brain FC is associated with impairment of the CC white matter in AgCC subjects; 3) stronger SC is generally associated with stronger FC.

2. Materials and methods

2.1. Participants

A total of 9 adults with AgCC [4 complete callosal agenesis, 3 callosal hypoplasia, 2 partial agenesis (frontal remnants, and lack of the body and splenium)], and 10 age-, gender-, and education-matched HC were included in our study. All study procedures were approved by the Ethics Committee of Beijing Chaoyang Hospital, Capital Medical University. Written informed consent was obtained from all participants. The following neuropsychological tests and scales were administered to all participants: the Mini-Mental State Exam (MMSE), the Montreal Cognitive Assessment (MoCA), the Hamilton Depression Rating Scale (HAM-D), and the Hamilton Anxiety Rating Scale (HAM-A).

2.2. Image acquisition

Image acquisition was performed on a Siemens 3.0 T scanner (MAGNETOM Trio-Tim, System AG, Germany) using a standard 8-channel head coil receiver at the Magnetic Resonance Center of Beijing Chaoyang Hospital, Capital Medical University.

Blood-oxygen-level-dependent (BOLD) fMRI data was acquired using a gradient-echo echo-planar imaging (EPI) sequence: repetition time (TR) = 2000 ms; echo time (TE) = 30 ms; flip angle = 90°; field of view (FOV) = 220 mm × 220 mm; image matrix = 64 × 64; slice thickness = 3 mm; in-plane voxel size = 3.4 × 3.4 × 3 mm^3; gap = 1 mm; 36 axial slices; with 178 volumes capturing the total period of brain activity of 6 min.

The whole-brain structural images were acquired using a magnetization-prepared rapid acquisition gradient-echo (MP-RAGE) T1-weighted sequence: TR = 1900 ms; TE = 2.52 ms; flip angle = 9°; total slices = 176; slice thickness = 1 mm; matrix = 250 × 250; in-plane voxel size = 1 × 1 × 1 mm^3.

The diffusion tensor imaging (DTI) data was acquired by axial, single-shot spin echo EPI sequence: TR = 7,700 ms; TE = 104 ms; flip angle = 90°; slice thickness = 3.5 mm; slice interval = 0 mm; total slices = 35; number of excitation = 2; scanning field = 230 × 230 mm; matrix = 128 × 128; in-plane voxel size = 1.8 × 1.8 × 3.5 mm^3; diffusion gradient duration (δ) = 21.2 ms; diffusion period (Δ) = 45.1 ms; diffusion gradient exerted at 20 directions with b = 1,000 s/mm^2, plus two b = 0 images covering the three-dimensional space of 230 × 230 × 122.5 mm^3.

2.3. Imaging data analyses

2.3.1. rs-fMRI data preprocessing

Rs-fMRI data was preprocessed with SPM12 software package (http://www.fil.ion.ucl.ac.uk/spm/), REST (http://restfmri.net/forum/rest) and Data Processing & Analysis of Brain Imaging (DPABI) (http://rfmri.org/dpabi) (Yan et al., 2016) on MATLAB R2015a (MathWorks) as follows: (1) removal of the first 10 volumes; (2) slice-timing correction; (3) head motion effects were regressed out used the Friston 24-parameter model (6 motion parameters, 6 temporal derivatives, and their squares); (4) coregistration of the T1 image to the mean rs-fMRI scans; (5) gray and white matter segmentation using “New Segment” and spatial normalization of the T1 image to a Montreal Neurological Institute (MNI) space using the DARTEL toolbox; (6) spatial normalization of the rs-fMRI data using the normalization parameters estimated in step 5 and voxel size resampling to 3 × 3 × 3 mm^3; (7) spatial smoothing with a Gaussian kernel of 4 mm full width at half maximum; (8) linearly detrended removal and temporal band-pass filtering within 0.01-0.1 Hz; and (9) regressing several nuisance covariates, including the global mean signal, white matter signal, and cerebrospinal fluid signal. Subjects with head motion correction, average head motion translation > 2 mm and/or rotation > 2° were removed.

2.3.2. Voxel-mirrored homotopic functional connectivity

VMHC assumes symmetric morphology between hemispheres. As this assumption does not hold for real brains, images must be transformed before VMHC can be calculated. Therefore, in our study anatomical and functional images were transformed to fit a symmetric template (Zuo et al., 2010) using the REST (http://restfmri.net/forum/rest) software. Lastly, VMHC was computed as the Pearson correlation of the BOLD time course between any pair of symmetric interhemispheric voxels.

2.3.3. Resting-state functional network analyses

To evaluate the overall network topology of FC in AgCC subjects, we

adopted a graph-theoretic approach (Hung et al., 2019). For the region of interest (ROI) based network analyses, the mean time course was extracted from 116 cortical and subcortical ROIs from the automatic anatomic labeling (AAL) atlas. Pearson correlation coefficients were computed between each pair of all 116 ROIs. Then, a Fisher r to z transformation was applied to improve the normality of these correlation coefficients. For each pair of seed regions within one hemisphere, the homotopic regions in the opposite hemisphere defined the intrahemispheric and interhemispheric networks, respectively. Compiling all of the correlation coefficients results in a 116 × 116 adjacency matrix that denotes the strength of the temporal coupling (edges) between each pair of regions (nodes).

FC matrices were binarized at various threshold (0.01:0.25) in the two groups. Based on these binarized matrices the following six commonly used graph-theory measurements were calculated by using Gretna Toolbox (Owen et al., 2013b; Wang et al., 2015): degree, small-worldness (Sigma), mean clustering coefficient (Gamma), shortest characteristic path length (Lambda), global efficiency (Eg), and local efficiency (Eloc) (Xia et al., 2013).

2.3.4. DTI data preprocessing

All the DTI images were preprocessed using Pipeline for Analysing braiN Diffusion imAges (PANDA) (https://www.nitrc.org/projects/panda/) (Cui et al., 2013). After head motion and eddy current corrections, each subject's DTI dataset was registered to the same individual's high-resolution structural image and then into the standard MNI space using affine transformations. Specifically, the FA map of each subject was calculated in native space and was affinely co-registered to its corresponding T1-weigted images. Then, T1-weighted images were nonlinearly registered to the MNI space. The inverse transformations were obtained to the above two steps to transform the AAL atlas from MNI space to diffusion native space. Lastly, a voxel-wise calculation of the tensor matrix yielded FA, mean diffusivity (MD), axial diffusivity (AD), and radial diffusivity (RD).

2.3.5. Deterministic tractography

A whole-brain deterministic tractography approach was performed using the fiber assignment by continuous tracking (FACT) algorithm (Mori et al., 1999). Fiber tracking was terminated at voxels where FA < 0.2 or where the angle between two eigenvectors was greater than 45°. The CC structure for each subject was manually traced on the T1 image and cross-validated on the FA image. FN and FA of the fibers crossing the CC were calculated for each subject and their correlation with VMHC was estimated.

2.3.6. Probabilistic tractography

Although deterministic tractography is suitable for the quantification of the white matter fibers of large structures like CC, it may underestimate the fiber numbers connecting two smaller brain regions and get false negative results, and it is difficult to capture crossing fibers within one voxel. Probabilistic tractography with Bayesian Estimation of Diffusion Parameters Obtained using Sampling Techniques (Bedpostx) (Behrens et al., 2007) can solve this problem. Hence, except for the quantification of FN and FA of the fibers crossing CC as mentioned above, all the following DTI analyses, including SC network construction, graph-based analysis of the SC network, and the CC structural network identification were performed with probabilistic tractography.

The Bedpostx runs Markov Chain Monte Carlo sampling to build up distributions on diffusion parameters at each voxel, and models crossing fibers within each voxel of the brain and automatically determines the number of crossing fibers per voxel, where the diffusion coefficient is modelled using a Gamma distribution. After Bedpostx estimation has been applied, we performed probabilistic tractography analyses. Briefly, the procedure produces sample streamlines, by starting from a seed and then iterating between (1) drawing an orientation from the voxel-wise Bedpostx distributions, (2) taking a step in this direction, and (3) checking for any termination criteria. 5000 streamlines were generated. These sample streamlines can then be used to build up a histogram of the number of streamlines connecting two brain regions. The SC value was estimated based on this streamline distribution, and was corrected by the length of streamlines. Hence, the SC value represents the normalized posterior probability of white matter connections between two brain areas.

T1-weighted MR images were automatically segmented using DARTEL (Ashburner and Friston, 2009). The 116 AAL regions were used as the seed points for the aforementioned probabilistic tractography. The resulting 116 × 116 SC matrix reflects the distribution of pairwise white matter connections, i.e. SC values, between nodes. The SC matrices were then used to assess the network properties. The network graph topology analysis was performed with the same procedure as the rs-fMRI data.

2.3.7. Identifying the corpus callosum structural network

To identify the structural connections that are highly reliant on the corpus callosum, namely "CC structural network", we first performed two probabilistic tractography analyses, one with and one without the CC mid-way point mask (as an "inclusion ROI" for probabilistic tractography) between each pair of the 116 brain regions of HC, respectively, then a percentage matrix was generated by the ratio between the matrixes achieved above, i.e. with/without the CC midpoint mask. Finally, the CC structural network was determined by the percentage matrix with the assumption that one connection is considered to be significantly relying on the CC if its percentage matrix value is higher than 90%.

2.3.8. Statistical analyses

To identify the differences in inter-hemispheric FC between the two groups, we performed two-sample t-tests on the VMHC maps (corrected $p < 0.05$ with voxel-level $p < 0.05$ and cluster size > 54 voxels, as determined by the AlphaSim correction (Song et al., 2011)).

We then extracted the mean VMHC values from the clusters showing significant differences between the two groups and correlated the mean VMHC values with the FN and FA values separately for the AgCC and HC groups. To further evaluate the dependence of interhemispheric FC on the CC structure in healthy condition, we performed a voxel-wise correlation analysis between the VMHC maps and FN/FA of fibers crossing the CC (FN/FA values obtained using deterministic tractography), across HC subjects.

We used two-sample t-tests to compare the Fisher z-transformed SC and FC matrices acquired from probabilistic tractography and rs-fMRI network analysis, respectively, as well as the SC matrices of the CC structural network (acquired from probabilistic tractography) between the AgCC and HC groups. To assess the statistical significance of group comparisons of SC metrics, we used a nonparametric permutation. For each metric, the data labels were randomly reassigned between the two groups and t values were computed for each relabeling, for a total of 5000 permutations. P values were calculated on the basis of the distribution of t values obtained from the permutations and were adjusted for multiple comparisons with an FDR correction. For statistical comparisons of the FC between groups, we utilized the Network-Based Statistics (NBS) method (Zalesky et al., 2010). A *t* test was applied to assess the statistical significance of between-group comparisons of the network metrics. A total of 10,000 permutations were performed to estimate the null distribution and associations with $t > 3$ were analyzed by NBS. An FWE-corrected significance level of $p < 0.01$ was used. The brain networks were visualized with the BrainNet Viewer for Matlab 2015a (Xia et al., 2013).

The five graph-theory based network measurements were compared between groups at different thresholds and a significant difference was accepted if the p value was less than 0.05 at each threshold. Age and gender were included in the model as covariates of nuisance.

Table 1
The demographics and the clinical characteristics of the AgCC subjects.

Cases	Case 1	Case 2	Case 3	Case 4	Case 5	Case 6	Case 7	Case 8	Case 9
Age	31	31	54	27	17	53	24	57	41
Gender	Female	Female	Female	Female	Female	Male	Male	Male	Male
Education	9	9	12	16	9	9	9	10	11
Handedness	Left	Left	Left	Right	Left	Right	Right	Right	Right
Type of dysgenesis	Partial	Complete	Partial	Complete	Hypoplasia	Complete	Complete	Hypoplasia	Hypoplasia
Probst bundle	Present	Present	Present	Present	Present	Present	Present	Present	Present
Sigmoid bundle	Present	Absent	Absent	Absent	Absent	Absent	Absent	Absent	Absent
MMSE	28	28	28	30	30	30			
MoCA	21	21	26	30	24	27			
HAMD	10	10	8	5	6	7			
HAMA	4	4	10	3	4	5			
Barthel Index	100	100	100	100	100	100	100	100	100
Brain malformation	No	Enlarged posterior horn of later ventricle	Large interhemispheric cyst	Large interhemispheric lipoma	Small cyst close to left ventricle	Enlarged posterior horn of later ventricle	Enlarged posterior horn of later ventricle	No	No

MMSE: Mini-mental state examination, MoCA: Montreal Cognitive Assessment, HAMD: Hamilton Depression Scale, HAMA: Hamilton Anxiety Scale.

In addition to calculating the correlation coefficient between the whole-brain SC (all the elements in the 116 × 116 SC matrix achieved by probabilistic tractography described in the section 2.3.6) and FC values (all the elements in the 116 × 116 FC matrix described in the section 2.3.3), we generated a two-dimensional histogram to visualize the relationship between SC and FC. The height of the histogram indicates the number of connections (edges) between pairs of brain regions (nodes), while the horizontal plane indicates the distribution of SC and FC. The same analysis was performed again across the connections within the CC network only, i.e. the connections that rely heavily on the CC structure. The mean SC and FC values of the connections within the CC structural network were compared between the AgCC and HC groups using two-sample t-tests.

Lastly, it is notable that the proportion of left-handed subjects in the AgCC group was higher than that in the controls, and some subjects also have brain malformations (Table 1). Therefore, we performed secondary analyses, i.e. repeated all the above analyses with handedness and brain malformations as covariates.

3. Results

3.1. The demographics and clinical data

The demographic, clinical, and neuroradiologic characteristics of AgCC are described in Table 1. There were no significant differences in mean age (37.2 ± 14.5 vs. 47.1 ± 13.0), education (10.4 ± 2.3 vs. 10.1 ± 3.8) and gender (4 males vs. 6 males) ($p > 0.05$) between the AgCC and HC groups. There were five right-handed and four left-handed individuals in AgCC group, however, while all the controls were right-handed. Both groups showed no evidence of any other neurological or neuropsychological disease. There were no significant differences in performance on neuropsychological tests between the two groups (Table 1). The T1-weighted MR images with midline sagittal view and the corresponding deterministic tractography of three representative subjects with three different types of AgCC and one control are presented in Fig. 1. Coronal and sagittal T1 images and the deterministic tractography files of all 9 AgCC patients are included in the Supplementary material.

There were also some malformations such as encephalomalacia, interhemispheric cysts, or lipomas presented in AgCC subjects. The Probst bundles were noted in all subjects using deterministic tractography (Table 1 and Fig. 1).

3.2. VMHC and its relationship with FN and FA of fibers crossing the CC

Subjects with AgCC showed significantly reduced homotopic VMHC compared to HC in 18 brain regions, including bilateral dorsolateral prefrontal cortex, middle frontal gyrus, lingual gyrus, postcentral gyrus, precentral gyrus, supplementary motor area, cingulum gyrus, precuneus and insula (Fig. 2A). By contrast, there was no increased VMHC in subjects with AgCC compared with HC. Furthermore, FN and FA of the fibers crossing the CC were estimated with deterministic tractography, and we found that there were significant correlations between VMHC with the FN (Fig. 2B and Fig. 2D) and FA (Fig. 2C and Fig. 2D) values of fibers crossing the CC in HC in the above areas, while there were no significant correlations in the AgCC group alone.

3.3. Network analyses of DTI and fMRI

Comparisons of the SC matrices between the AgCC and HC groups revealed increased intrahemispheric, but decreased interhemispheric SC in AgCC (Fig. 3A, left panel). Intrahemispheric connections between parietal, frontal, and subcortical areas showed increased SC, while decreased SC was seen between homotopic areas such as bilateral sensorimotor areas, insula, frontal, and occipital areas, as well as between asymmetric interhemipsheric areas in AgCC (Fig. 3A, right panel). Decreased mean degrees in AgCC subjects were found in the bilateral middle frontal gyrus, posterior cingulate gyrus, precuneus and thalamus; right dorsolateral superior frontal gyrus, calcarine, postcentral gyrus and caudate nucleus; left cuneus, middle occipital gyrus and caudate nucleus. However, there was no increased degree in AgCC subjects compared to HC.

Comparisons of the FC matrices between the AgCC and HC groups revealed different patterns from the SC analysis (Fig. 3B, left panel). Increased or decreased FC areas were scattered across the brain rather than concentrated within or between hemispheres. AgCC subjects showed significantly decreased FC between parietal, frontal, and occipital areas, while areas with increased FC were mainly isolated edges (connections) that did not form a circuit or network and therefore did not survive the NBS correction. The decreased degrees were mainly located in the right precentral gyrus, left supplementary motor area, and right precuneus in AgCC subjects compared to the controls. However, increased degrees were located in the left subcortical regions, including left hippocampus, amygdala, putamen, and pallidum (Fig. 3B, lower right panel).

Graph-based network analyses showed that as threshold increased, Sigma, Gamma, and Lambda increased, while Eg, and Eloc decreased in both structural and functional networks (Fig. 4). Area-under-the-curve (AUC) of the threshold was provided for these indices within the threshold range in Table 2. Graph-based network analyses of the SC data showed impaired global properties in AgCC subjects (lower in global efficiency as well as higher in characteristic path length and

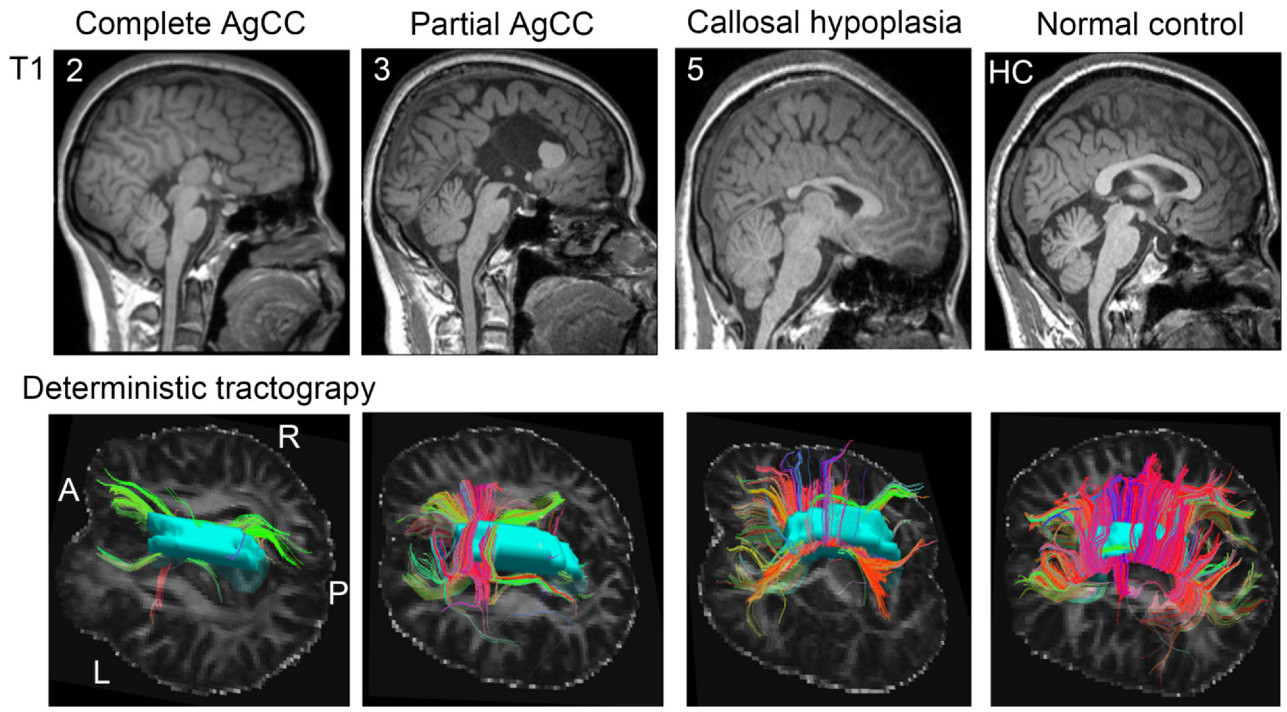

Fig. 1. T1-weighted MR images with midline sagittal view and the corresponding deterministic tractography of four representative subjects. Three types of AgCC (the first column is patient no. 2 with complete AgCC, the second column is patient no. 3 with partial AgCC, the third column is patient no. 5 with callosal hypoplasia) and one healthy control (the fourth column) are presented. In the lower panel, an axial slice of the FA image was used as the background. A normal complete corpus collosum (CC) structure is shown by the cyan color. Colored streamlines represent white matter fibers crossing the CC structure. Spatial marks indicate the orientation of the 3D image, anterior (A), posterior (P), left (L), and right (R). (For interpretation of the references to color in this figure legend, the reader is referred to the web version of this article.)

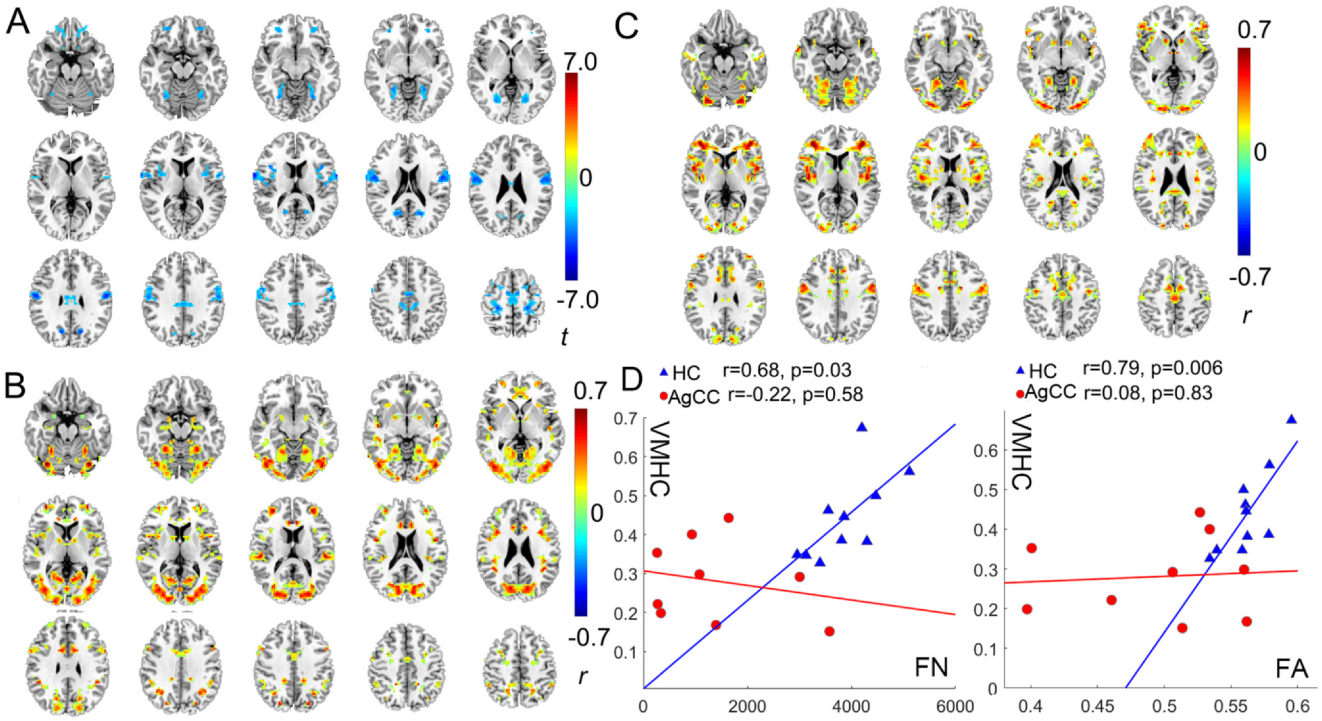

Fig. 2. Abnormal VMHC in AgCC and the correlations between VMHC and FN/FA of the fibers crossing the corpus callosum. Decreased VMHC in AgCC compared to HC (A). Voxel-wise correlation analyses between VMHC and FN (B) as well as FA (C) across HC, indicate that ordinarily there is strong, shared correlation between VMHC and FN/FA values for the bilateral postcentral gyrus, precentral gyrus, supplementary motor area, cingulum gyrus, precuneus, insula, dorsolateral prefrontal cortex, middle frontal gyrus, and lingual gyrus in healthy subjects. The FA and FN values used in the above analyses were determined from the fiber tracts crossing the CC as generated via deterministic tractography. (D) VMHC correlated with the values of FN/FA in HC (blue), however, there was no correlation in the AgCC group alone (red). (For interpretation of the references to color in this figure legend, the reader is referred to the web version of this article.)

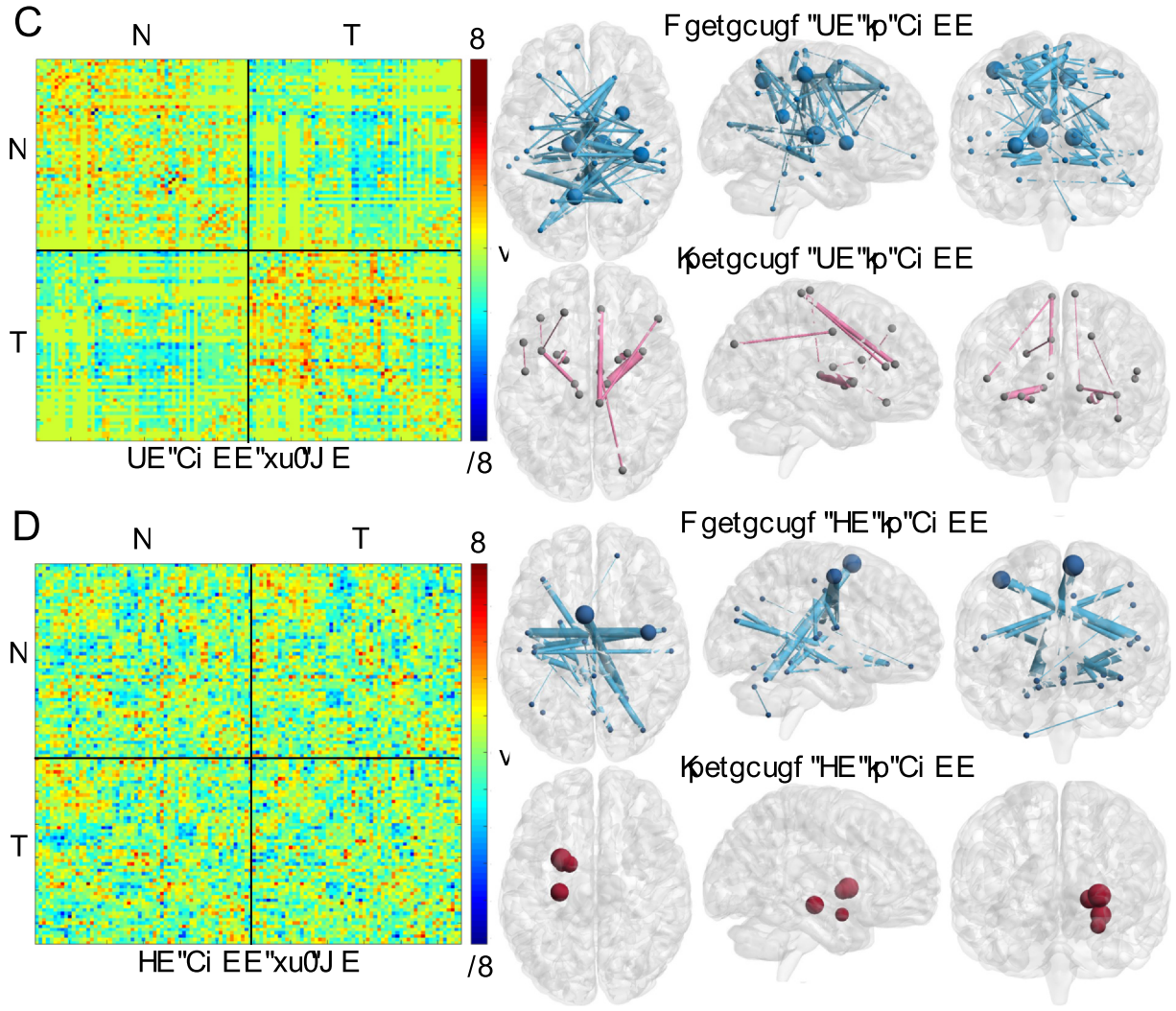

Fig. 3. Comparisons of whole brain structural (A, upper panel) and functional connectivity (B, lower panel) between AgCC subjects and HC. In the left panel of both subfigures of (A) and (B), the 116 by 116 t-value matrix represents the group difference of SC/FC matrices between AgCC subjects and HC. Left and right hemisphere brain regions were separated in the matrix. In the right panel, the above view, left-side view, and front view of the brain are displayed, the thickness of the edges in the brain maps represent the significance of difference of the SC (A) or FC (B) connections between AgCC and HC, and the size of the spheres indicate the difference in degrees of nodes between AgCC and HC subjects.

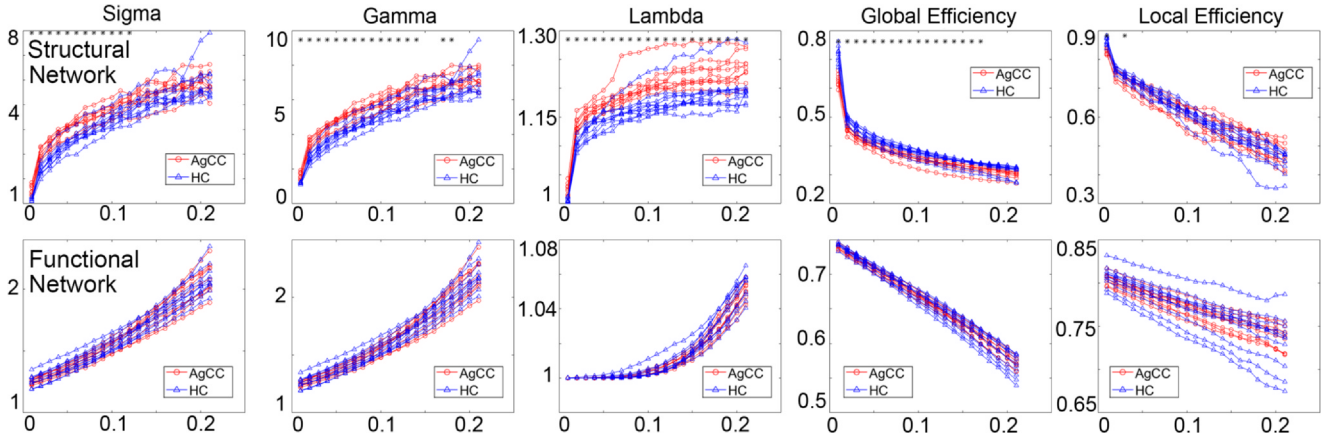

Fig. 4. Graph-theory based network topology properties of structure network and functional network in AgCC subjects and HC. The five graph-theory based network measurements were compared between AgCC (red) and HC (blue) subjects at different thresholds for structural network (upper row) and functional network (lower row), respectively. Each line represents one subject. The asterisks (*) above indicate significant differences ($p < 0.05$) in corresponding graph-theory measurement at each threshold. Structural network topological analyses indicates disruptions in the global connectivity (Sigma, Gamma, Lambda, Global efficiency) while local connectivity (Local efficiency) remains generally unaffected. At any threshold, there were no significant differences in functional network measurements between AgCC subjects and HC. (For interpretation of the references to color in this figure legend, the reader is referred to the web version of this article.)

Table 2
Structural and functional network topological properties of the AgCC and HC subjects.

Network metrics of rs-fMRI	AgCC	HC	T values	P values
Global efficiency	0.132 ± 0.001	0.132 ± 0.002	−0.189	0.852
Local efficiency	0.154 ± 0.002	0.154 ± 0.004	−0.866	0.399
Clustering coefficient	0.109 ± 0.004	0.109 ± 0.008	−1.009	0.328
Characteristic path length	0.305 ± 0.003	0.306 ± 0.004	−1.224	0.904
Small world	0.324 ± 0.011	0.324 ± 0.010	−5.000	0.623
Network metrics of DTI				
Global efficiency	0.073 ± 0.002	0.077 ± 0.003	−3.901	**0.001***
Local efficiency	0.121 ± 0.005	0.121 ± 0.005	−0.385	0.705
Clustering coefficient	0.086 ± 0.004	0.086 ± 0.002	0.574	0.574
Characteristic path length	0.564 ± 0.022	0.535 ± 0.021	4.358	**0.0005***
Small world	0.952 ± 0.054	0.879 ± 0.068	1.758	**0.031***

* Denotes significantly different from Control group ($p < 0.05$).

small world index). However, no significant differences in the local properties (i.e. local efficiency and mean clustering coefficient) were found between the two groups (Fig. 4). Graph-based network analysis of the FC data showed no significant difference at any density level for the network measures of the matrices including global efficiency, local efficiency, clustering coefficient, characteristic path length and small world properties (such as sigma, lambda and gamma) (Table 2 and Fig. 4).

3.4. The relationship between structural and functional connectivity

By contrasting the probabilistic tractography with and without the CC midpoint mask, we identified the white matter connections that heavily rely on the CC in HC (Fig. 5, upper panel). This CC structural network (Fig. 5, lower left) connects not only with homotopic areas such as the bilateral primary sensory/motor areas, frontal, occipital, and temporal areas, but also with those asymmetric inter-hemispheric components such as connections from the limbic/subcortical areas to the contralateral parietal, frontal, and motor areas. As expected, SC was significantly decreased within the CC structural network in the AgCC group ($p < 0.001$) (Fig. 5, lower right).

A two-dimensional histogram of whole brain connections showed that when the SC values are low, the FC values are evenly split between positive and negative. As SC increases, the FC tends to become more positive (Fig. 6A, upper panel). The same relationship exists within the CC structural network (Fig. 6A, lower panel). It is notable that although the same number of streamlines were generated for each ROI, the total number of connections crossing through the CC (height of the histograms) is significantly lower in the AgCC compared to the HC ($t = 4.01$, $p < 0.001$). Scatter plots also showed significant positive correlations between whole brain SC and FC values in HC ($r = 0.22$, $p < 0.001$) and AgCC ($r = 0.21$, $p < 0.001$), as well as between the SC and FC that reliant on the corpus callosum in HC ($r = 0.15$, $p < 0.001$) and AgCC ($r = 0.10$, $p < 0.001$) (Fig. 6B, left). The mean SC values within the CC structural network are significantly lower in the AgCC group than that of HC ($t = -3.84$, $p < 0.001$) (Fig. 6B, middle). However, there was no significant difference in the FC values within the CC structural network between the two groups ($t = -0.35$, $p = 0.86$) (Fig. 6B, right).

Including handedness and brain malformation information as additional covariates did not change any of the results above significantly.

4. Discussion

We report three major findings. First, AgCC subjects showed markedly reduced VMHC compared to HC. The VMHC was significantly correlated with the quantity and quality of the fibers crossing the CC structure in normal brains. Second, structural network analyses revealed impaired global properties (decreased global efficiency, small world index, and mean degree, increased characteristic path length and mean betweenness), but relatively intact local properties (clustering coefficient and local efficiency) in AgCC subjects compared to controls. We did not find significant differences in functional network properties between the two groups. Third, in both AgCC subjects and controls, brain areas with more fiber connections are more likely to demonstrate a positive FC with each other, while brain areas with fewer white matter connections are more likely to have negative FC.

4.1. Dependence of interhemispheric FC on corpus callosum

The extent to which interhemispheric FC depends on the CC is uncertain, and previous studies have offered contradictory evidence (Uddin, 2013). The occurrence of bilaterally symmetric independent components in the AgCC group together with intact global functional network properties demonstrates unambiguously that interhemispheric functional integration can exist in the absence of structural connectivity (Tyszka et al., 2011). Evidence from electroencephalography (EEG) studies also show that there are no significant differences in any frequency band between homologous pairs of electrodes between subjects that have undergone a corpus callostomy and those with an intact CC (Casimo et al., 2018). Thus, changes in functional connectivity in AgCC may not be severe enough to be detectable by those approaches.

Our study demonstrates that VMHC (Zuo et al., 2010), which quantifies the FC between each voxel in one hemisphere and its mirrored counterpart in the other, is a more sensitive method for detecting abnormality in AgCC cases. The VMHC was significantly decreased in the sensorimotor, visual, and frontal areas in the AgCC subjects compared to the HC, suggesting that the CC is important for VMHC in these areas. Previous studies also found that the VMHC values vary from region to region (Zuo et al., 2010). Primary sensorimotor cortices associated with large and fast callosal fibers present higher VMHC, while associative cortices, characterized by small and slow axons, have relatively lower VMHC (Zuo et al., 2010). These observations in our current study are consistent with a previous report (Stark et al., 2008). All of these evidences reflect the relationship between VMFC and anatomical features of white matter tracts of CC: faster conduction fibers are likely to produce tighter synchronization of neurophysiological signals.

To what extent would the CC structure be related to the degree of functional integration across hemispheres as indexed by VMHC? This question was tested by correlating the robustness of the CC bundles with the VMHC values. Strikingly, the dependency of VMHC on the CC structure was more significant in the HC group alone, but not significant in the AgCC group (Fig. 2). The tight link between the CC structural connection and VMHC in HC suggests that normally the interhemispheric neural synchrony is dependent on the quantity and quality of the fibers of CC. While both structural and functional connections between two hemispheres decreased dramatically in AgCC patients. Compensatory side pathways, intrahemispheric structural connections, the symmetry of cerebral blood perfusion, and other physiological factors likely affect the interhemispheric FC values in AgCC subjects, and may explain the lack of correlation between VMHC and FN/FA in AgCC.

4.2. Increased intrahemispheric structural/functional connections as compensatory mechanisms in AgCC

Recent work on structural connectivity in adults and children with AgCC has shown that the absence of long-range interhemispheric callosal fibers results in reduced information transmission and integration between the cerebral hemispheres (Jakab et al., 2015; Meoded et al., 2015; Owen et al., 2013b). Additionally, increased local structural connectivity and a more segregated network organization have been

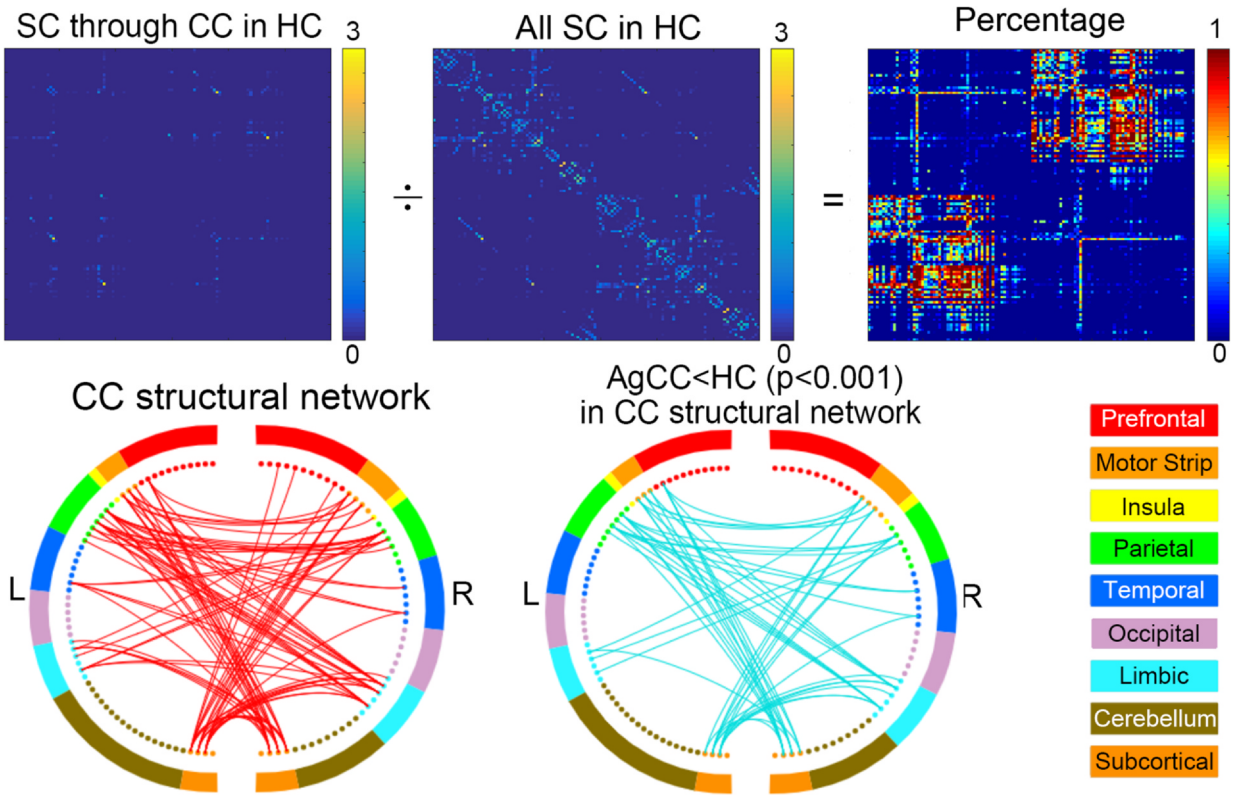

Fig. 5. The structural connections crossing the corpus callosum. Upper panel shows the SC matrix in healthy controls generated from probabilistic tractography with (matrix on the left) and without (matrix in the middle) the CC as the mid-way point, as well as the percentage matrix (right) calculated by dividing the two matrices. The percentage matrix quantifies the proportion of fibers that go through the CC structure among all the fibers connecting each pair of the regions. A connection is considered to be significantly reliant on the CC if this percentage is higher than 90. Based on the above definition, the structural connections that rely heavily on the CC structure in HC are presented in the lower left panel, and the changes of connections in AgCC subjects compared to HC are presented in the lower right panel. All structural connections relying heavily on the CC structure in AgCC subjects were significantly decreased.

observed in these subjects (Meoded et al., 2015; Owen et al., 2013b). Some evidence for white matter circuit reorganization in AgCC has been reported (Tovar-Moll et al., 2007; Wahl et al., 2009), but no rewiring of any kind has been identified in adults subjected to a callosal transection or "split brain" operation. Congenital agenesis of the CC permits developmental adaptive reorganization (Paul, 2011), therefore, individuals without a CC from birth frequently exhibit less severe symptoms of disconnection syndrome. Whole-brain probabilistic fiber tracking in the current study revealed significantly decreased interhemispheric SC, but increased intrahemispheric fiber connections in the AgCC subjects. The SC small-worldness, clustering coefficients, and global efficiency were also higher in the AgCC subjects than in HC. These results may likely reflect the profound rearrangement of cortical and subcortical connectivity within the cerebral hemispheres due to the formation of pre- and postnatal structural compensatory mechanisms.

The published literature and our current results indicate that a normal complement of resting-state networks and intact functional coupling between the hemispheres can emerge in the absence of the CC. Although the FC between some brain areas decreased significantly, there was no significant decrease in the global and local functional efficiency in the AgCC group. We even observed increased FC degrees in the left hippocampus, amygdala, putamen, and pallidum. These increased FC are consistent with our DTI findings of increased white matter connections between the subcortical limbic areas and cortical areas in AgCC. Previous studies also indicated that the compensatory FC in AgCC individuals was associated with enhanced cerebral plasticity during childhood, possibly allowing the recruitment of alternative neural structures to enable interhemispheric communication through the subcortical structures, anterior, intercollicular, or posterior commissures (Beaule et al., 2015), such as the previously described Probst and sigmoid bundles (Jakab et al., 2015; Tovar-Moll et al., 2014). The enhanced FC in AgCC is unilateral in the left limbic area. It has been reported that the subcortical limbic regions in the left and right hemispheres typically show differentiated asymmetric functional activities in normal subjects (Raemaekers et al., 2018). A recent study with normal subjects also found that brain areas with fewer callosal connections were more likely to develop lateralized functions (Karolis et al., 2019), Therefore, the AgCC subjects may develop lateralized asymmetric functional pathways to compensate for the possibility of impairments in language, movement, and social communication functions. The unilateral changes of FC in AgCC, might be associated with the dominant role of the left hemisphere in the above processing (Hodgson and Hudson, 2018; Raemaekers et al., 2018), Further studies with paradigms targeting unilateral hemisphere specialization are required to examine brain functional lateralization. In our present study, there were no significant differences in performance on neuropsychological tests between the two groups, and the finding fits with the functional imaging evidence, which confirmed that subjects with AgCC might have acquired the compensatory neural plasticity for maintaining these functions (Tovar-Moll et al., 2014). Taken together, the increased intrahemispheric SC and FC serves as an important compensatory mechanism and helps to maintain basic brain function in AgCC individuals. These evidences highlight the importance of heterotopic connectivity of the CC and ipsilateral associative pathways that help distribute information within each hemisphere (Roland et al., 2017).

The divergent results from SC and FC network analyses indicate that although SC contributes to FC, it only partially shapes functional organization which is consistent with the expected greater number and flexibility of functional networks as compared to structural networks that is noted in earlier studies.

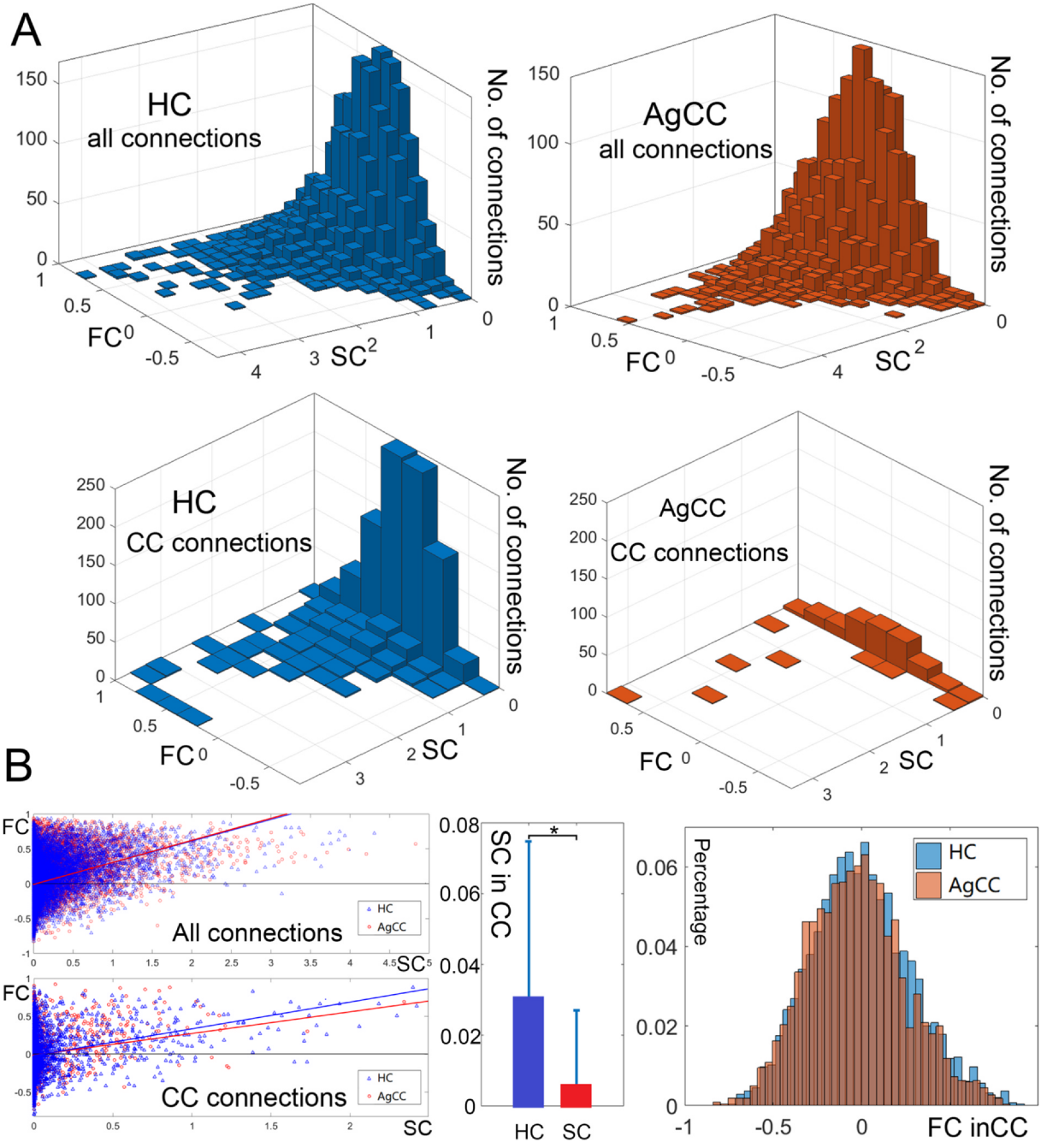

Fig. 6. The relationship between structural and functional connectivities. (A) Two-dimensional histogram of the distribution of whole brain SC and FC (upper row) in HC (blue) and AgCC subjects (orange), and the distribution of SC and FC between the corpus callosum (CC) connected brain areas (lower row). The height of the histogram indicates the number of connections (edges) between pairs of brain regions (nodes), while the horizontal plane indicates the distribution of SC and FC. (B) Left, scatter plots with trendlines revealed significant correlation between SC and FC, both among whole brain connections and the connections which heavily rely on the CC, in HC (blue) and AgCC (red) subjects. Middle, the mean SC values of the connections which heavily rely on the CC in HC are significantly higher than that of AgCC subjects. Right, the distributions of FC values of the connections which rely on the CC are not significantly different between HC and AgCC subjects. (For interpretation of the references to color in this figure legend, the reader is referred to the web version of this article.)

4.3. The structural basis for the positive and negative FC

Although the distribution of SC and FC values across the whole brain are similar between AgCC and HC (Fig. 6 A first row), the total number of connections crossing through the CC is lower in the AgCC compared to the HC, indicating that there is a significant loss of CC connections in the AgCC condition, and it mainly affects the inter-hemispheric SC rather than global SC.

FC has been widely used in studying normal brain function and neuropathological changes in various brain diseases. However, the structural basis for positive or negative FC is still unknown. To the best of our knowledge, this is the first study to quantify the dependency of FC on the SC. Our results showed that brain areas with stronger SC (higher fiber density and larger FA) were more likely to have a positive FC. This phenomenon was seen in both HC and AgCC groups. Probabilistic tractography with the CC as mid-way point showed that the functional connectivities were not always positive for those brain areas that were mainly connected by the CC structure, as some of them showed negative FC. However, brain areas with more fiber connections showed positive FC and brain areas with fewer fiber connections

showed negative FC. Abnormal correlation or anti-correlation between different brain networks has been proposed as a potential neural biomarker for certain diseases, such as major depressive disorders, autism, bipolar disorders, and schizophrenia. The current study may help us to further understand the structural basis for diminished anti-correlation or abnormal FC in these diseases and inspire the development of new treatments that can modify the fiber connections between certain brain areas.

Although FC is known to largely reflect patterns of SC (Meier et al., 2016), the former is not entirely predictable on the basis of the latter (Uddin, 2013). It is usually found to exceed it (Damoiseaux and Greicius, 2009). For example, in this study, the presence of strong SC is predictive of FC, but strong FC could still be detected between what appear to be structurally unconnected regions. This non-linear relationship between SC and FC is thought to reflect the complexity of FC that arises from indirect polysynaptic pathways or due to multiple external driving forces. Therefore, both structural and functional connectivity should be considered as complementary approaches to investigate the human connectome at a large-scale level.

One of limitations of our study was notable; the proportion of left-handed subjects in AgCC group was higher than that in the HC group, which might be due to a compensatory mechanism for the disconnected homotopic motor areas. Unfortunately, we couldn't examine the exact mechanism behind this interesting phenomenon because of the low number of subjects. The major goal of the current study was to examine the relationship between SC and FC, and we did not find statistically significant differences between including and excluding the handedness as a covariate, indicating that the main effects of group difference and the correlations (for instance, FC and SC) were much stronger than the effect of handedness.

In summary, our study revealed the important role of the CC structure in maintaining interhemispheric FC and clarified the general relationship between structural and functional connectivities, using AgCC as a model. These results can provide new insights into the underlying neurological pathophysiology of brain malformations and thereby also help elucidate the structure–function relationship of the normal human brain.

Funding

This work was supported by the National Natural Science Foundation of China (81301016) and the Beijing Municipal Administration of Hospitals Incubating Program (PX2019009); and NIH grants: R21MH114020, R01MH114982, K24MH104449.

CRediT authorship contribution statement

Junliang Yuan: Conceptualization, Data curation, Formal analysis, Investigation, Visualization, Writing - original draft, Writing - review & editing, Resources, Funding acquisition. **Xiaopeng Song:** Conceptualization, Data curation, Formal analysis, Investigation, Methodology, Software, Visualization, Validation, Writing - original draft, Writing - review & editing. **Elliot Kuan:** Writing - original draft, Writing - review & editing. **Shuangkun Wang:** Data curation, Writing - review & editing, Resources. **Long Zuo:** Data curation, Writing - review & editing, Resources. **Dost Ongur:** Conceptualization, Writing - review & editing, Supervision, Project administration, Resources, Funding acquisition. **Wenli Hu:** Writing - review & editing, Resources, Funding acquisition. **Fei Du:** Conceptualization, Writing - original draft, Writing - review & editing, Supervision, Project administration, Resources, Funding acquisition.

Declaration of Competing Interest

The authors declare that they have no known competing financial interests or personal relationships that could have appeared to influence the work reported in this paper.

Acknowledgements

We would like to thank Dr. Suyu Zhong, and Dr. Zaixu Cui for their valuable suggestions and assistance in data processing.

Appendix A. Supplementary data

Supplementary data to this article can be found online at https://doi.org/10.1016/j.nicl.2020.102425.

References

Ashburner, J., Friston, K.J., 2009. Computing average shaped tissue probability templates. Neuroimage 45, 333–341.
Beaule, V., Tremblay, S., Lafleur, L.P., Tremblay, S., Lassonde, M., Lepage, J.F., Theoret, H., 2015. Cortical thickness in adults with agenesis of the corpus callosum. Neuropsychologia 77, 359–365.
Behrens, T.E., Berg, H.J., Jbabdi, S., Rushworth, M.F., Woolrich, M.W., 2007. Probabilistic diffusion tractography with multiple fibre orientations: What can we gain? Neuroimage 34, 144–155.
Biswal, B.B., 2012. Resting state fMRI: a personal history. Neuroimage 62, 938–944.
Calabrò, R.S., Spadaro, L., Marra, A., Balletta, T., Cammaroto, S., Bramanti, P., 2015. Agenesis of corpus callosum and frontotemporal dementia: a casual finding? Am. J. Alzheimer's Disease Other Dementias 30, 375–379.
Casimo, K., Grassia, F., Poliachik, S.L., Novotny, E., Poliakov, A., Ojemann, J.G., 2018. Preservation of electrophysiological functional connectivity after partial corpus callosotomy: case report. J. Neurosurg. Pediatr. 22, 214–219.
Cui, Z., Zhong, S., Xu, P., He, Y., Gong, G., 2013. PANDA: a pipeline toolbox for analyzing brain diffusion images. Front. Hum. Neurosci. 7, 42.
Damoiseaux, J.S., Greicius, M.D., 2009. Greater than the sum of its parts: a review of studies combining structural connectivity and resting-state functional connectivity. Brain Struct. Funct. 213, 525–533.
Hodgson, J.C., Hudson, J.M., 2018. Speech lateralization and motor control. Prog. Brain Res. 238, 145–178.
Honey, C.J., Sporns, O., Cammoun, L., Gigandet, X., Thiran, J.P., Meuli, R., Hagmann, P., 2009. Predicting human resting-state functional connectivity from structural connectivity. Proc. Natl. Acad. Sci. U.S.A. 106, 2035–2040.
Hung, S.C., Lee, C.C., Chen, H.H., Chen, C., Wu, H.M., Lin, C.P., Peng, S.J., 2019. Early recovery of interhemispheric functional connectivity after corpus callosotomy. Epilepsia 60, 1126–1136.
Jakab, A., Kasprian, G., Schwartz, E., Gruber, G.M., Mitter, C., Prayer, D., Schopf, V., Langs, G., 2015. Disrupted developmental organization of the structural connectome in fetuses with corpus callosum agenesis. Neuroimage 111, 277–288.
Karolis, V.R., Corbetta, M., Thiebaut de Schotten, M., 2019. The architecture of functional lateralisation and its relationship to callosal connectivity in the human brain. Nat. Commun. 10, 1417.
Kozel, F.A., Rao, U., Lu, H., Nakonezny, P.A., Grannemann, B., McGregor, T., Croarkin, P.E., Mapes, K.S., Tamminga, C.A., Trivedi, M.H., 2011. Functional connectivity of brain structures correlates with treatment outcome in major depressive disorder. Front. Psychiatry 2.
Le Bihan, D., Mangin, J.F., Poupon, C., Clark, C.A., Pappata, S., Molko, N., Chabriat, H., 2001. Diffusion tensor imaging: concepts and applications. J. Magnetic Resonance Imaging 13, 534–546.
Mancuso, L., Costa, T., Nani, A., Manuello, J., Liloia, D., Gelmini, G., Panero, M., Duca, S., Cauda, F., 2019. The homotopic connectivity of the functional brain: a meta-analytic approach. Sci. Rep. 9, 3346.
Meier, J., Tewarie, P., Hillebrand, A., Douw, L., van Dijk, B.W., Stufflebeam, S.M., Van Mieghem, P., 2016. A Mapping Between Structural and Functional Brain Networks. Brain Connect. 6, 298–311.
Meoded, A., Katipally, R., Bosemani, T., Huisman, T.A., Poretti, A., 2015. Structural connectivity analysis reveals abnormal brain connections in agenesis of the corpus callosum in children. Eur. Radiol. 25, 1471–1478.
Miguel-Hidalgo, J.J., 2013. Brain structural and functional changes in adolescents with psychiatric disorders. Int. J. Adolescent Med. Health 25, 245–256.
Mori, S., Crain, B.J., Chacko, V.P., van Zijl, P.C., 1999. Three-dimensional tracking of axonal projections in the brain by magnetic resonance imaging. Ann. Neurol. 45, 265–269.
O'Reilly, J.X., Croxson, P.L., Jbabdi, S., Sallet, J., Noonan, M.P., Mars, R.B., Browning, P.G.F., Wilson, C.R.E., Mitchell, A.S., Miller, K.L., Rushworth, M.F.S., Baxter, M.G., 2013. Causal effect of disconnection lesions on interhemispheric functional connectivity in rhesus monkeys. Proc. Natl. Acad. Sci. U.S.A. 110, 13982–13987.
Owen, J.P., Li, Y.O., Yang, F.G., Shetty, C., Bukshpun, P., Vora, S., Wakahiro, M., Hinkley, L.B., Nagarajan, S.S., Sherr, E.H., Mukherjee, P., 2013a. Resting-state networks and the functional connectome of the human brain in agenesis of the corpus callosum. Brain Connect. 3, 547–562.
Owen, J.P., Li, Y.O., Ziv, E., Strominger, Z., Gold, J., Bukhpun, P., Wakahiro, M., Friedman, E.J., Sherr, E.H., Mukherjee, P., 2013b. The structural connectome of the human brain in agenesis of the corpus callosum. Neuroimage 70, 340–355.

Park, H.-J., Friston, K., 2013. Structural and functional brain networks: from connections to cognition. Science (New York, N.Y.) 342.
Paul, L.K., 2011. Developmental malformation of the corpus callosum: a review of typical callosal development and examples of developmental disorders with callosal involvement. J. Neurodev. Disord. 3, 3–27.
Paul, L.K., Brown, W.S., Adolphs, R., Tyszka, J.M., Richards, L.J., Mukherjee, P., Sherr, E.H., 2007. Agenesis of the corpus callosum: genetic, developmental and functional aspects of connectivity. Nat. Rev. Neurosci. 8, 287–299.
Raemaekers, M., Schellekens, W., Petridou, N., Ramsey, N.F., 2018. Knowing left from right: asymmetric functional connectivity during resting state. Brain Struct. Funct. 223, 1909–1922.
Ridley, B., Beltramone, M., Wirsich, J., Le Troter, A., Tramoni, E., Aubert, S., Achard, S., Ranjeva, J.-P., Guye, M., Felician, O., 2016. Alien Hand, Restless Brain: Salience Network and Interhemispheric Connectivity Disruption Parallel Emergence and Extinction of Diagonistic Dyspraxia. Front. Hum. Neurosci. 10.
Roland, J.L., Snyder, A.Z., Hacker, C.D., Mitra, A., Shimony, J.S., Limbrick, D.D., Raichle, M.E., Smyth, M.D., Leuthardt, E.C., 2017. On the role of the corpus callosum in interhemispheric functional connectivity in humans. Proc. Natl. Acad. Sci. U.S.A. 114, 13278–13283.
Song, X.W., Dong, Z.Y., Long, X.Y., Li, S.F., Zuo, X.N., Zhu, C.Z., He, Y., Yan, C.G., Zang, Y.F., 2011. REST: a toolkit for resting-state functional magnetic resonance imaging data processing. PLoS ONE 6, e25031.
Stark, D.E., Margulies, D.S., Shehzad, Z.E., Reiss, P., Kelly, A.M., Uddin, L.Q., Gee, D.G., Roy, A.K., Banich, M.T., Castellanos, F.X., Milham, M.P., 2008. Regional variation in interhemispheric coordination of intrinsic hemodynamic fluctuations. J. Neurosci. 28, 13754–13764.
Straathof, M., Sinke, M.R., Dijkhuizen, R.M., Otte, W.M., 2019. A systematic review on the quantitative relationship between structural and functional network connectivity strength in mammalian brains. J. Cerebral Blood Flow Metabolism 39, 189–209.
Tovar-Moll, F., Moll, J., de Oliveira-Souza, R., Bramati, I., Andreiuolo, P.A., Lent, R., 2007. Neuroplasticity in human callosal dysgenesis: a diffusion tensor imaging study. Cereb. Cortex 17, 531–541.
Tovar-Moll, F., Monteiro, M., Andrade, J., Bramati, I.E., Vianna-Barbosa, R., Marins, T., Rodrigues, E., Dantas, N., Behrens, T.E., de Oliveira-Souza, R., Moll, J., Lent, R., 2014. Structural and functional brain rewiring clarifies preserved interhemispheric transfer in humans born without the corpus callosum. Proc. Natl. Acad. Sci. U.S.A. 111, 7843–7848.
Tyszka, J.M., Kennedy, D.P., Adolphs, R., Paul, L.K., 2011. Intact bilateral resting-state networks in the absence of the corpus callosum. J. Neurosci. 31, 15154–15162.
Uddin, L.Q., 2013. Complex relationships between structural and functional brain connectivity. Trends Cogn. Sci. 17, 600–602.
Wahl, M., Strominger, Z., Jeremy, R.J., Barkovich, A.J., Wakahiro, M., Sherr, E.H., Mukherjee, P., 2009. Variability of homotopic and heterotopic callosal connectivity in partial agenesis of the corpus callosum: a 3T diffusion tensor imaging and Q-ball tractography study. AJNR Am. J. Neuroradiol. 30, 282–289.
Wang, J., Wang, X., Xia, M., Liao, X., Evans, A., He, Y., 2015. GRETNA: a graph theoretical network analysis toolbox for imaging connectomics. Front. Hum. Neurosci. 9 386-386.
Wang, J., Zuo, X., He, Y., 2010. Graph-based network analysis of resting-state functional MRI. Front. Syst. Neurosci. 4, 16.
Xia, M., Wang, J., He, Y., 2013. BrainNet Viewer: a network visualization tool for human brain connectomics. PLoS ONE 8, e68910.
Yan, C.G., Wang, X.D., Zuo, X.N., Zang, Y.F., 2016. DPABI: Data Processing & Analysis for (Resting-State) Brain Imaging. Neuroinformatics 14, 339–351.
Zalesky, A., Fornito, A., Bullmore, E.T., 2010. Network-based statistic: identifying differences in brain networks. Neuroimage 53, 1197–1207.
Zuo, X.N., Kelly, C., Di Martino, A., Mennes, M., Margulies, D.S., Bangaru, S., Grzadzinski, R., Evans, A.C., Zang, Y.F., Castellanos, F.X., Milham, M.P., 2010. Growing together and growing apart: regional and sex differences in the lifespan developmental trajectories of functional homotopy. J. Neurosci. 30, 15034–15043.